3562 *Chem. Mater.* **2009,** *21,* 3562–3569
DOI:10.1021/cm901161g

CHEMISTRY OF MATERIALS
Article

Facile Synthesis of Three-Dimensional Dendritic Platinum Nanoelectrocatalyst

Liang Wang[†] and Yusuke Yamauchi*[,†,‡]

[†]*World Premier International Research Center, International Center for Materials Nanoarchitectonics, National Institute for Materials Science, Namiki 1-1, Tsukuba, Ibaraki, 305-0044 Japan, and* [‡]*PRESTO, Japan Science and Technology Agency, 4-1-8 Honcho, Kawaguchi, 332-0012 Japan*

Received January 26, 2009

Design and synthesis of three-dimensional (3D) dendritic platinum nanostructures (DPNs), with its advantages of high surface area, low density, and reduced materials costs represent a highly interesting class of materials. In this paper, a very simple and efficient wet chemical route to straightforward synthesis of well-dispersed 3D DPNs at high yield was proposed, which was carried out by simply mixing K_2PtCl_4 aqueous solution and poly(vinyl pyrrolidone) (PVP) at a constant 30 °C for 1 h in the presence of ascorbic acid (AA). As-prepared 3D DPNs were highly porous, self-supporting nanostructures that possessed high surface area and supply enough absorption sites for reactant molecules and were shown to be active as nanoelectrocatalyst for the reduction of dioxygen and oxidation of methanol.

1. Introduction

Morphology-controlled synthesis of metal nanostructures has attracted considerable interests.[1] It is generally accepted that the morphology (including dimensionality and shape) of the nanostructures can effectively tune their intrinsic chemical and physical properties, e.g., tailoring the catalytic properties of a functional materials.[1] Among various metal nanostructures, nanostructured platinum is of particular interest because of its unique catalytic properties.[2] For instance, nanostructured platinum serves as a major catalyst in the industrial synthesis of nitric acid, reduction of pollutant gases emitted from automobiles, oil cracking, and proton exchange membrane (PEM) fuel cells.[3] The manipulation of the size and shape of platinum materials at the nanoscale can contribute to lowering Pt usage and achieving the necessary cost reduction.[4] Up to date, much effort has focused on the development of techniques to produce Pt catalyst with a high surface area to achieve high catalytic performance and utilization efficiency.[5]

A range of technically important platinum nanostructures with specific structural features, such as nanospheres,[6] nanofibers,[7] nanowire,[4a,8] nanotubes,[9] nanosheets,[10] nanowheels,[11] nanocages,[12] nanodendrites,[13] etc., have been successfully prepared by various strategies including templated and templatless synthesis. The synthesis of specific nanostructured platinum with high surface area is highly desirable and potentially technologically important. For instance, design and synthesis of hollow Pt nanostructures, with its advantages of high surface area, low density, and reduced materials costs represent a highly interesting class of materials.[14] Platinum hollow nanospheres have been prepared by the nanoparticles templating

*Corresponding author. E-mail: Yamauchi.Yusuke@nims.go.jp.

(1) (a) Burda, C.; Chen, X. B.; Narayanan, R.; El-Sayed, M. A. *Chem. Rev.* **2005**, *105*, 1025. (b) Wiley, B.; Sun, Y. G.; Xia, Y. N. *Acc. Chem. Res.* **2007**, *40*, 1067. (c) Ramirez, E.; Eradès, L.; Philippot, K.; Lecante, P.; Chaudret, B. *Adv. Funct. Mater.* **2007**, *17*, 2219. (d) Xie, J. P.; Lee, J. Y.; Wang, D. I. C. *Chem. Mater.* **2007**, *19*, 2823.
(2) (a) Xiong, Y. J.; Wiley, B. J.; Xia, Y. N. *Angew. Chem., Int. Ed.* **2007**, *46*, 7157. (b) Guo, Y. G.; Hu, J. S.; Wan, L. J. *Adv. Mater.* **2008**, *20*, 2878. (c) Lee, I.; Morales, R.; Albiter, M. A.; Zaera, F. *Proc. Natl. Acad. Sci. U.S.A.* **2008**, *105*, 15241. (d) Lu, J.; Do, I.; Drzal, L. T.; Worden, R. M.; Lee, I. *ACS Nano* **2008**, *2*, 1825. (e) Ge, X. B.; Wang, R. Y.; Liu, P. P.; Ding, Y. *Chem. Mater.* **2007**, *19*, 5827.
(3) (a) Roucoux, A.; Schulz, J.; Patin, H. *Chem. Rev.* **2002**, *102*, 3757. (b) Chen, J.; Herricks, T.; Geissler, M.; Xia, Y. *J. Am. Chem. Soc.* **2004**, *126*, 10854.
(4) (a) Song, Y. J.; Garcia, R. M.; Dorin, R. M.; Wang, H. R.; Qiu, Y.; Coker, E. N.; Steen, W. A.; Miller, J. E.; Shelnutt, J. A. *Nano Lett.* **2007**, *7*, 3650. (b) Lim, B.; Lu, X. M.; Jiang, M. J.; Camargo, P. H. C.; Cho, E. C.; Lee, E. P.; Xia, Y. N. *Nano Lett.* **2008**, *8*, 4043.
(5) (a) Chen, J. Y.; Herricks, T.; Xia, Y. N. *Angew. Chem., Int. Ed.* **2005**, *44*, 2589. (b) Sun, S. H.; Yang, D. Q.; Villers, D.; Zhang, G. X.; Sacher, E.; Dodelet, J. P. *Adv. Mater.* **2008**, *20*, 571. (c) Tian, N.; Zhou, Z. Y.; Sun, S. G.; Ding, Y.; Wang, Z. L. *Science* **2007**, *316*, 732. (f) Wang, C.; Daimon, H.; Onodera, T.; Koda, T.; Sun, S. H. *Angew. Chem., Int. Ed.* **2008**, *47*, 3588.
(6) Bigall, N. C.; Hartling, T.; Klose, M.; Simon, P.; Eng, L. M.; Eychmuller, A. *Nano Lett.* **2008**, *8*, 4588.
(7) Yamauchi, Y.; Takai, A.; Nagaura, T.; Inoue, S.; Kuroda, K. *J. Am. Chem. Soc.* **2008**, *130*, 5426.
(8) Sun, S. H.; Jaouen, F.; Dodelet, J. P. *Adv. Mater.* **2008**, *20*, 3900.
(9) Kijima, T.; Yoshimura, T.; Uota, M.; Ikeda, T.; Fujikawa, D.; Mouri, S.; Uoyama, S. *Angew. Chem., Int. Ed.* **2004**, *43*, 228.
(10) (a) Peng, X. S.; Luo, Y. H.; Jin, J.; Huang, J. G.; Ichinose, I.; Kurashima, K.; Papadimitrakopoulos, F. *Chem. Commun.* **2006**, 4688. (b) Song, Y. J.; Steen, W. A.; Peña, D.; Jiang, Y. B.; Medforth, C. J.; Huo, Q.; Pincus, J. L.; Qiu, Y.; Sasaki, D. Y.; Miller, J. E.; Shelnutt, J. A. *Chem. Mater.* **2006**, *18*, 2335.
(11) Song, Y. J.; Dorin, R. M.; Garcia, R. M.; Jiang, Y. B.; Wang, H. R.; Li, P.; Qiu, Y.; Swol, F.; Miller, J. E.; Shelnutt, J. A. *J. Am. Chem. Soc.* **2008**, *130*, 12602.
(12) Song, Y. J.; Garcia, R. M.; Dorin, R. M.; Wang, H. R.; Qiu, Y.; Shelnutt, J. A. *Angew. Chem., Int. Ed.* **2006**, *45*, 8126.
(13) Wang, H. R.; Song, Y. J.; Medforth, C. J.; Shelnutt, J. A. *J. Am. Chem. Soc.* **2006**, *128*, 9284.
(14) (a) Mayers, B.; Jiang, X.; Sunderland, D.; Cattle, B.; Xia, Y. *J. Am. Chem. Soc.* **2003**, *125*, 13364. (b) Garcia, R. M.; Song, Y. J.; Dorin, R. M.; Wang, H. R.; Li, P.; Qiu, Y.; Swol, F.; Shelnutt, J. A. *Chem. Commun.* **2008**, 2535.

Published on Web 07/16/2009

method, which involves a galvanic replacement reaction between sacrificial nanoparticles and a platinum complex.[15] Mesoporous platinum with highly ordered networks and narrow pore-size distributions is another interesting material. Mesoporous platinum have been prepared by the chemical or electrochemical reduction of platinum salts dissolved in aqueous lyotropic liquid crystals (LLC) made of nonionic surfactants at high concentrations.[16] Recently, we have proposed the facile approach to the rational synthesis of mesoporous Pt based on the LLC template.[16b−f] The main process is formation of LLC and subsequent reduction of the platinum complex dissolved in aqueous phases in LLC.

Despite the above successful demonstrations such as hollow and mesoporous Pt nanostructures, it remains a grand challenge to produce three-dimensional (3D) Pt nanostructures, together with well-controlled dimensions and morphologies, such as Pt nanostructures with 3D dendritic morphology, which are highly porous, self-supporting nanostructures that possess a high degree of electrical connectivity because of their dendritic morphology.[10b] Such 3D dendritic platinum nanostructures (DPNs) can decrease the Pt consumption, provide high surface area and supply more absorption sites for reactant molecules with increased performance in catalytic applications. The synthesis of 3D DPNs is a fairly recent development. To date, only several examples of the preparation of Pt nanostructures with 3D dendritic morphology are demonstrated and these synthesis are not easy.[17] For example, based on sonoelectrochemical reduction of platinum complex, Zhu et al. synthesized 3D DPNs;[18] Ullah et al. prepared CTAB-stabilized 3D DPNs, which were selectively synthesized depending upon the pH values of 1.7 of the synthetic aqueous solutions;[19] very recently, Chang et al. produced Pt nanodendrites from the reduction of $PtCl_6^{2-}$ ions via galvanic replacement reactions with Te nanowires at 90 °C.[17e]

The straightforward synthesis of 3D DPNs via a simple wet chemical route is still highly desirable to date, which can potentially create new opportunities for making a high-performance catalyst. Herein, a one-step and efficient wet chemical route to straightforwardly synthesize well-dispersed 3D DPNs at high yield was proposed. Furthermore, the as-prepared 3D DPNs were shown to be active as a nanoelectrocatalyst in the dioxygen reduction and methanol oxidation.

2. Experimental Section

2.1. Typical Synthesis of 3D DPNs. In a typical synthesis, 5 mL of 20 mM K_2PtCl_4 aqueous solution and powdery poly(vinyl pyrrolidone) (PVP) (K-30, M_w 40 000) with the initial molar ratios of 1:3.5 were placed in a small beaker, and then 5 mL of 0.1 M ascorbic acid (AA) was added. Aging of the K_2PtCl_4 solution was not needed in this synthetic procedure. After the solution was sonicated for 1 min at room temperature, the temperature of the solution was kept constant at 30 °C for 1 h. The color of the reaction solution changed within 40 min from transparent light brownish-yellow (from the Pt complex) to brownish-gray (slowly), then to opaque black (quickly). Residual PVP polymer was removed by centrifuge at 8000 rpm for 15 min. The collected product was redispersed in water with sonicating to produce a stable colloid solution and stored at ambient condition for characterization.

2.2. Synthesis of ~6 nm Pt Nanoparticles. Six nanometer Pt nanoparticles were prepared by reduction of H_2PtCl_6 aqueous solution with trisodium citrate according to ref 20. Briefly, 1 mL of 1% H_2PtCl_6 aqueous solution was added into 100 mL of water and then the solution was heated to boiling. Aging of the H_2PtCl_6 solution was not necessary in this synthetic procedure. Then, 3 mL of 1% sodium citrate aqueous solution was added rapidly, and the mixture was kept at a boiling temperature for about 30 min. TEM was used to examine particle size distribution, and an average diameter of 6 nm of Pt colloids was confirmed (data not shown).

2.3. Characterizations. Transmission electron microscope (TEM) and high-resolution transmission electron microscope (HRTEM) were carried out using a JEOL JEM-2100F operated at 200 kV equipped with energy dispersive spectrometer (EDS) analyses. The sample for TEM and HRTEM characterization was prepared by placing a drop of sample solution on a carbon-coated copper grid and dried at room temperature. High-angle powder X-ray diffraction (XRD) patterns were obtained with a Rigaku Rint 2500X diffractometer with monochromated Cu Kα radiation (40 kV, 100 mA) operated by using a step scan program (step width 0.05°). Nitrogen adsorption and desorption data were obtained by using a Belsorp 28 apparatus (Bel Japan, Inc.) at 77 K, and the sample was heated at 50 °C for 24 h before the measurement.

2.4. Electrocatalytic Investigations. Cyclic voltammograms (CVs) experiments were performed by using a CHI 832 electrochemical analyzer (CHI Instrument, U.S.). A conventional three-electrode cell was used, including a Ag/AgCl (saturated KCl) electrode as reference electrode, a platinum wire as counter electrode, and a working electrode. The working electrode included a bare Pt bulk electrode (3 mm in diameter, purity 99.99%), a glassy carbon electrode (GCE) (3 mm in diameter), or modified GCE, for different cases. The modified GCE was loaded with either as-parpared 3D DPNs or conventional ~6 nm Pt nanoparticles with the same Pt loadings of 4.2 μg and

(15) (a) Liang, H. P.; Zhang, H. M.; Hu, J. S.; Guo, Y. G.; Wan, L. J; Bai, C. L. *Angew. Chem., Int. Ed.* **2004**, *43*, 1540. (b) Chen, H. M.; Liu, R. S.; Lo, M. Y.; Chang, S. C.; Tsai, L. D.; Peng, Y. M.; Lee, J. *J. Phys. Chem. C* **2008**, *112*, 7522.
(16) (a) Attard, G. S.; Bartlett, P. N.; Coleman, N. R. B.; Elliott, J. M.; Owen, J. R.; Wang, J. H. *Science* **1997**, *278*, 838. (b) Yamauchi, Y.; Sugiyama, A.; Morimoto, R.; Takai, A.; Kuroda, K. *Angew. Chem., Int. Ed.* **2008**, *47*, 5371. (c) Takai, A.; Yamauchi, Y.; Kuroda, K. *Chem. Commun.* **2008**, 4171. (d) Yamauchi, Y.; Takai, A.; Komatsu, M.; Sawada, M.; Ohsuna, T.; Kuroda, K. *Chem. Mater.* **2008**, *20*, 1004. (e) Yamauchi, Y.; Momma, T.; Fuziwara, M.; Nair, S. S.; Ohsuna, T.; Terasaki, O.; Osaka, T.; Kuroda, K. *Chem. Mater.* **2005**, *17*, 6342. (f) Yamauchi, Y.; Kuroda, K. *Chem. Asian J.* **2008**, *3*, 664. (g) Choi, K. S.; McFarland, E. W.; Stucky, G. D. *Adv. Mater.* **2003**, *15*, 2018.
(17) (a) Zhong, X. H.; Feng, Y. Y.; Lieberwirth, I.; Knoll, W. *Chem. Mater.* **2006**, *18*, 2468. (b) Wang, L.; Guo, S. J.; Zhai, J. F.; Dong, S. J. *J. Phys. Chem. C* **2008**, *112*, 13372. (c) Song, Y.; Yang, Y.; Medforth, C. J.; Pereira, E.; Singh, A. K.; Xu, H.; Jiang, Y.; Brinker, C. J.; Swol, F.; Shelnutt, J. A. *J. Am. Chem. Soc.* **2004**, *126*, 635. (d) Teng, X. W.; Liang, X. Y.; Maksimuk, S.; Yang, H. *Small* **2006**, *2*, 249. (e) Lin, Z. H.; Lin, M. H.; Chang, H. T. *Chem.—Eur. J.* **2009**, *15*, 4656.
(18) Shen, Q. M.; Jiang, L. P.; Zhang, H.; Min, Q. H.; Hou, W. H.; Zhu, J. J. *J. Phys. Chem. C* **2008**, *112*, 16385.
(19) Ullah, M. H.; Chung, W. S.; Kim, I.; Ha, C. S. *Small* **2006**, *2*, 870.
(20) (a) Wang, L.; Guo, S. J.; Huang, L. J.; Dong, S. J. *Electrochem. Commun.* **2007**, *9*, 827. (b) Huang, M. H.; Shao, Y.; Sun, X. P.; Chen, H. J.; Liu, B. F.; Dong, S. J. *Langmuir* **2005**, *21*, 323.

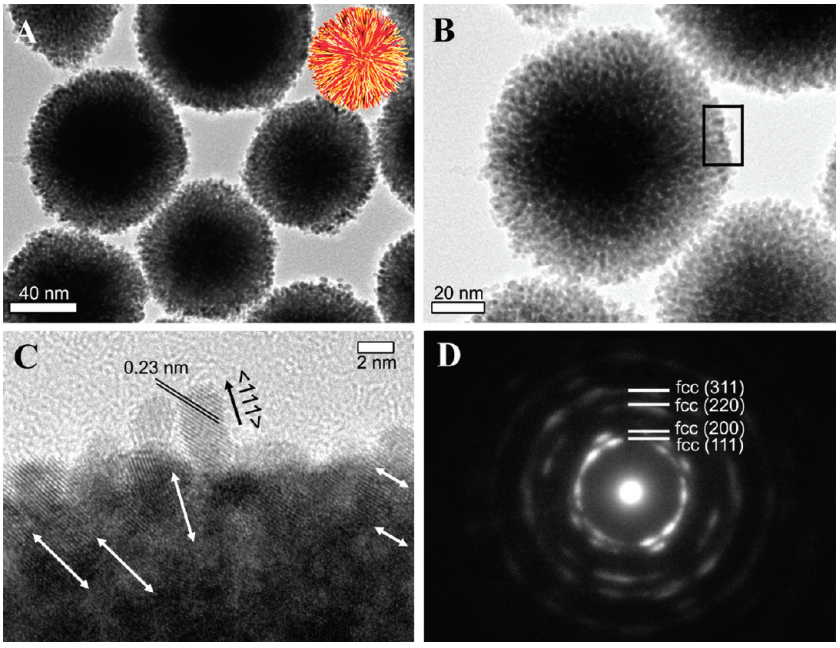

Figure 1. Typical TEM images of the well-dispersed 3D DPNs prepared by the typical synthesis at (A) lower- and (B) higher-magnification; (C) HRTEM image of the square area in panel B and (D) the SAED patterns. The inset in (A) shows a picture of a Koosh ball.

dried at room temperature. The electrode was then coated with 3 μL of 0.5% Nafion solution. Prior to electrochemical investigation, the bare Pt electrode and bare GCE were polished with diamond pastes and an alumina slurry down to 0.05 μm on a polishing cloth (Buehler, Lake Bluff, IL), followed by sonicating in water, ethanol, and water, respectively. The bare Pt electrode was then electrochemically cleaned by cycling the electrode potential between −0.2 and 1.6 V (vs Ag/AgCl) in 0.5 M H_2SO_4 until the CVs characteristic for a clean Pt electrode was obtained.

Electrocatalytic dioxygen reduction measurements were carried out in O_2-saturated or N_2-saturated 0.5 M H_2SO_4 solution at the scan rate of 50 mV s^{-1}. A RRDE-3 (ALS Co. Ltd.) was used for rotating disk electrode (RDE) and rotating ring-disk electrode (RRDE) experiments. A modified rotating glassy carbon disk-platinum ring electrode (diameter 5 mm) was used as working electrode. The collection efficiency (N) of the ring electrode obtained by reducing ferricyanide at the disk electrode was 0.21. Methanol electrocatalytic oxidation measurements were carried out in 0.5 M H_2SO_4 solution containing 1 M methanol and the scan rate was 50 mV s^{-1}.

In electrocatalytic investigations, electrochemical active surface area (ECSA) of each electrode was used to normalize the current density. ECSA of the Pt-based working electrodes were determined by integrating the amount of charge of the hydrogen adsorption and desorption peaks in the CVs (0.5 M H_2SO_4, 200 mV s^{-1}) over the time and by assuming that the charge density of a monolayer hydrogen adsorption/desorption on smooth platinum surface amounts to 210 μC cm^{-2}.[16g] The ECSA of the bare GCE were determined on the basis of the charge associated with the oxidation and reduction of 5 mM $K_3Fe(CN)_6$ containing 1 M KCl, which was calculated on the basis of the Randles−Sevcik equation, assuming mass transport only by the diffusion process[2d]

$$I_p = 2.69 \times 10^5 A D^{1/2} n^{3/2} \gamma^{1/2} C$$

where n is the number of electrons participating in the redox reaction, D is the diffusion coefficient of the molecule (equal to $(6.70 \pm 0.02) \times 10^{-6}$ cm^2/s), C is the concentration of the probe molecule in the solution (mol/cm^3), and γ is the scan rate ($V\ s^{-1}$). ECSA of the used bare GCE was 0.062 cm^2.

3. Results and Discussion

3.1. Synthesis and Characterization of 3D DPNs. TEM images of the typical synthesized 3D DPNs were shown in Figure 1. The image obtained at lower magnification image (Figure 1A) indicated that the Pt nanostructures were well-dispersed as individual spherical entities appeared to be 3D complex nanodendrites, and strikingly uniform in morphology. No other platinum nanostructures were observed, demonstrating the high yield formation of the 3D DPNs. Higher magnification image (Figure 1B) displayed well-oriented 3D DPNs with the surface packed by highly assembled dendritic feelers branching in various directions. It was clear that the basic Pt dendritic feelers had relatively uniform diameters along their lengths. Figure 1C showed the HRTEM image of the area indicated by the square in Figure 1B, indicating that the dendritic feelers grew along the ⟨111⟩ direction. The lattice spacing between the (111) planes, 0.23 nm, was in agreement with that of the Pt bulk crystal.[3b] The lattice fringes were coherently extended across over several dendritic feelers, indicated by the arrows in Figure 1C. Therefore, selected-area electron diffraction (SAED) patterns of the spherical nanodendrites were not bright concentric rings, but the ring patterns with intense spots (Figure 1D). These rings were attributable to (111), (200), (220), and (311) Pt face-centered-cube (fcc) crystal diffractions. This confirmed that the 3D DPNs synthesized by this method were crystallized in a phase similar to bulk Pt.[5b,8] The dendritic nature of the 3D DPNs was more evident in the images obtained by scanning TEM using a high-angle annular dark-field (HAADF) (Figure 2A).

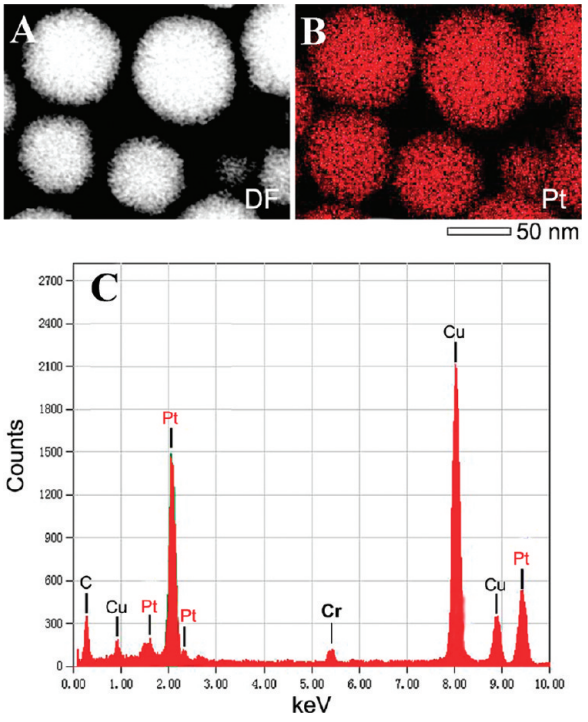

Figure 2. (A) HAADF scanning TEM image, (B) X-ray maps, and (C) EDX analysis of the 3D DPNs.

Specially, the nanoarchitectures of the3D DPNs could be kept even after strong sonication for 10 min or boiling for half an hour. Therefore, it might be considered that the complex nanodendrites were not the simple accumulation of the small nanounit. As shown by the inset of Figure 1A, the spherical nanodendrites superficially resemble nanoscale versions of common toys called "Koosh balls".

The chemical composition of the obtained 3D DPNs was determined by EDX analysis of the samples coated on the TEM grids. The EDX spectrum testified the existing of the Pt element, in which the peaks of the corresponding element Pt were distinct (other peaks originated from the copper, carbon and chromium signals from the TEM grid) (Figure 2C). From the corresponding X-ray maps (Figure 2B), it was revealed that the Pt element was distributed according to the morphology of the Pt nanostructures. These results clearly indicated that the as-prepared 3D DPNs were composed exclusively of metallic platinum. The XRD pattern of the product was as expected for fcc Pt crystal structure (Figure 3) consistent with the selected area electron diffraction (SAED) pattern of the sample (Figure 1D). In particular, the peaks attributed to the (111), (200), (220), and (311) reflections exhibited broadenings consistent with the nanoscale structural features seen by TEM (Figure 1A−C).[4a]

The surface area of the 3D DPNs was measured in order to demonstrate their potential uses as catalytic materials. Analysis of isotherms of the 3D dendritic nanostructures, as shown in Figure 4A, gave a surface area of 26 $m^2\ g^{-1}$. This value was very close to that of the commercial Pt catalyst (JM HiSPEC 1000, surface area: 27 m^2/g). For comparison, porous Pt nanoparticles

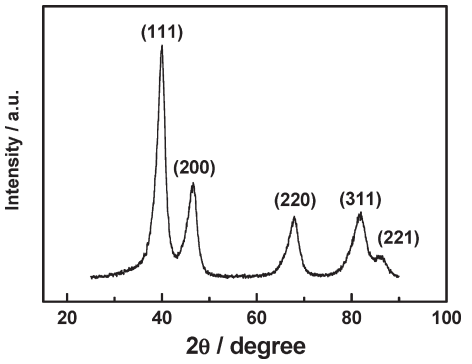

Figure 3. High-angle XRD pattern of the 3D DPNs.

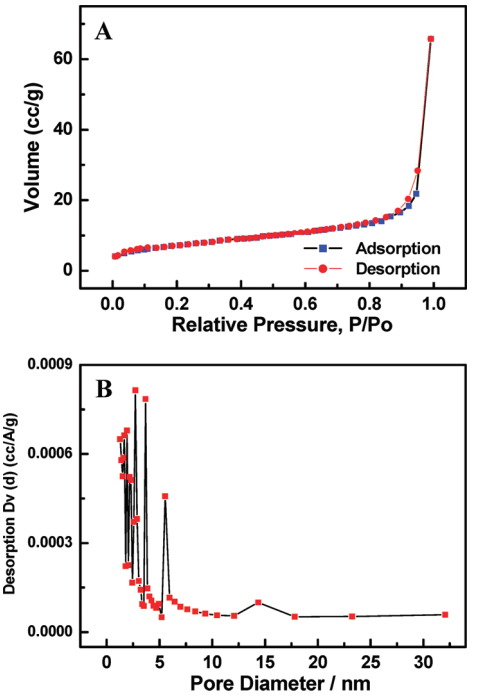

Figure 4. (A) N_2 adsorption−desorption isotherm of the 3D DPNs and (B) the pore-size distribution curve obtained from BJH method.

prepared by using complicated organic phase possessed a surface area of 14 $m^2\ g^{-1}$.[17d] Therefore, our synthetic strategy can be proposed as a more simple, straightforward and efficient wet chemical route for synthesis of 3D DPNs with high surface areas.

The pore-size distribution was further investigated by using the Barrett−Joyner−Halenda (BJH) method. BJH pore-size analysis gave a random distribution of pore sizes ranging from 1 to 17 nm, dominating distribution of pore sizes was within 1 to 5.5 nm (Figure 4B) and the broadness of the distribution indicated that the pores were not well-defined. These pores most likely corresponded to the naovoid space of the densely packed dendritic feelers networks observed in the TEM images (Figure 1B). The combination of high surface area with the nanoarchitecture consisting of pores (supplying great number of edges and absorption sites) is advantageous for catalytic applications.

The used amount of platinum precursor was apparently one of the key factors in the synthesis of the 3D

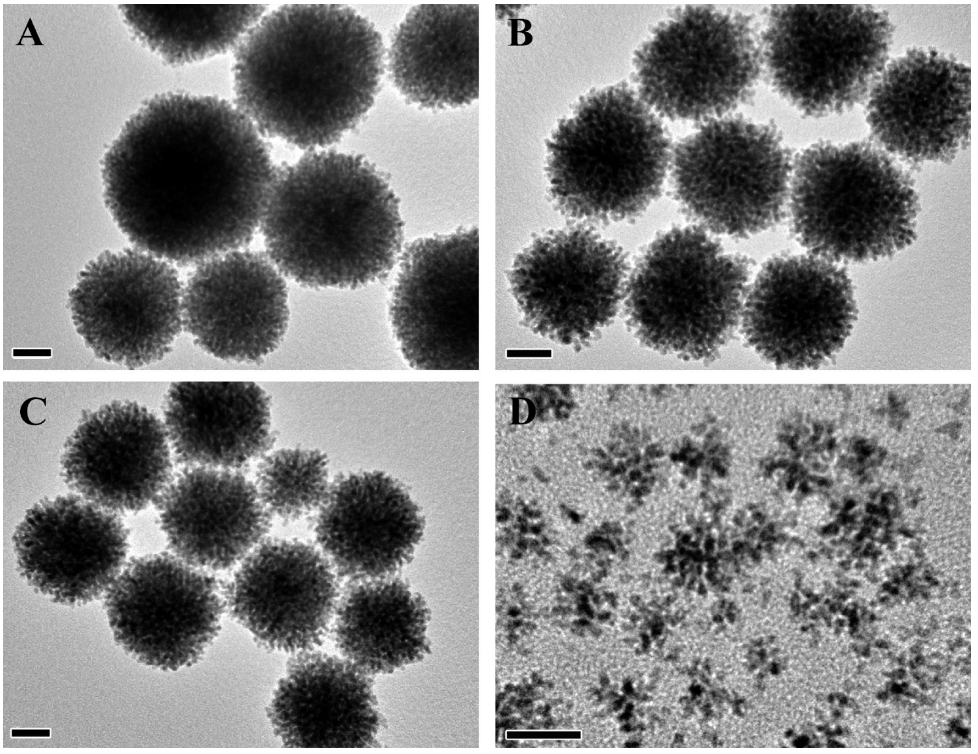

Figure 5. Typical TEM images of the Pt nanostructures prepared by different platinum precursor concentrations: (A) 15, (B) 10, (C) 5, and (D) 1 mM, respectively, under the identical conditions used for preparing typical 3D DPNs. The scale bar for each panel is 20 nm.

DPNs. Figure 5 showed typical TEM images of the Pt nanostructures prepared by different platinum precursor concentrations under the identical conditions used for preparing typical 3D DPNs. As shown in Figures 5A−C, well-dispersed dendritic Pt nanostructures could also be obtained when the platinum precursor concentrations ranged from 15 to 5 mM, and the dendritic morphology of the product was kept highly uniform. Figure 5D revealed, when the Pt precursor concentration further decreased to 1 mM, no similar 3D DPNs could be produced and only lots of Pt nanostructures with various sizes were obtained. Interestingly, the morphologies of the Pt nanostructures appeared in Figure 5D were, to some extent, similar to the newly prepared Pt multiarmed nanostar which was recently reported by El-Sayed et al.[21] It was very difficult to examine the morphological time evolution of the 3D DPNs. The Pt^{II} species were reduced at a very slow rate at the beginning stage in the proposed approach and the color of the solution kept transparent light brownish-yellow until a sudden change to brownish-gray, and then soon to opaque black.

A mechanism based on slow, continuous nucleation (seeding) and fast autocatalytic growth has previously been used to explain the growth of metallic nanoparticles,[22] especially Pt nanodendrites.[3b,17c,17d] A related mechanism is proposed to explain the formation of the platinum nanodendrites in the present work. In this proposed process, platinum ions were slowly reduced by AA and formed Pt nanoclusters growth centers (seeds). Once the seeds reached the certain size (about 500 atoms), the reduction of platinum ions was accelerated through an autocatalytic reduction process, which would be facilitated to a highly anisotropic mode to form single-crystal Pt dendritic feelers on the surface of each nanoclusters,[3b] and then rapidly grow into the mature nanostructures shown in Figure 1A−C as the autocatalytic reduction exhausted the available platinum complex. The slow, continuous formation of seed nanoparticles over the entire reaction, combining with the variation in the autocatalytic growth period for seed particles produced at different times, leads to a broad size distribution.[17c,17d] This mode of formation might explain the growth mechanism of 3D DPNs. However, the detailed formation mechanism of the 3D DPNs in this synthesis is not very clear at the present time and needs further investigation.

3.2. Electrocatalysis of the 3D DPNs toward Dioxygen Reduction and Methanol Oxidation. As displayed in Figure 6, the current densities in the hydrogen adsorption/desorption and oxide formation/reduction regions increased in the order of bulk Pt electrode, 6 nm Pt nanoparticles, and 3D DPNs, indicating that the 3D DPNs possessed larger ECSA and might lead to achieve higher catalytic performance. For comparison, the ECSAs of the two used Pt nanostructures, the ECSAs were $22.1 \pm 2\,cm^2\,g^{-1}$ and $8.5 \pm 2\,cm^2\,g^{-1}$ for the 3D DPNs and 6 nm Pt nanoparticles, respectively.

It is highly interesting to exploring the as-prepared 3D DPNs as a nanoelectrocatalyst. The oxygen reduction reaction (ORR) is a reaction of indispensable importance

(21) Mahmoud, M. A.; Tabor, C. E.; El-Sayed, M. A.; Ding, Y.; Wang, Z. L. *J. Am. Chem. Soc.* **2008**, *130*, 4590.
(22) Watzky, M. A.; Finke, R. G. *J. Am. Chem. Soc.* **1997**, *119*, 10382.

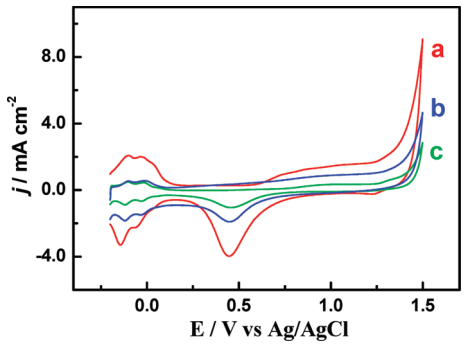

Figure 6. ECAS-normalized CVs of (a) 3D DPNs and (b) 6 nm Pt nanoparticle modified glassy carbon electrode, and (c) bulk Pt electrode, respectively, in N_2-saturated 0.5 M H_2SO_4. The scan rate was 100 mV s^{-1}.

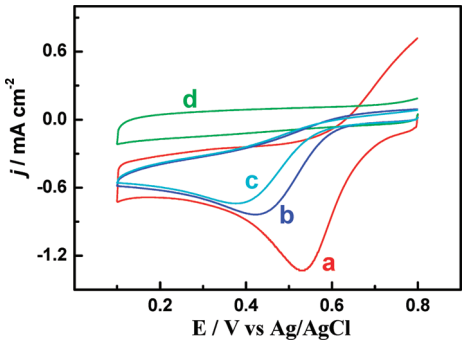

Figure 7. ECAS-normalized CVs in O_2-saturated 0.5 M H_2SO_4 with (a) 3D DPNs, (b) 6 nm Pt nanoparticles, and (c) bulk Pt electrode. (d) For comparison, ECAS-normalized CV of 3D DPNs in N_2-saturated 0.5 M H_2SO_4 is also shown. Scan rate was 50 mV s^{-1}.

in metal−air batteries and fuel cells as well as in oxygen sensors.[23] The electroreduction of dioxygen usually requires high current density, low overpotential, and nearly synchronous delivery of four electrons. The electrocatalytic properties of the 3D DPNs toward the ORR were tested and compared with approximate 6 nm Pt nanoparticles and bulk Pt electrode. As demonstrated in Figure 7, when 3D DPNs modified GCE used in O_2-saturated 0.5 M H_2SO_4 for ORR (Figure 7a), a remarkable catalytic reduction current occurred at 0.53 V and no catalytic reduction current was observed in the presence of N_2 (Figure 7d), indicating that the catalytic current located at 0.53 V was ascribed to the reduction of oxygen. It was also shown in Figure 7 that the 3D DPNs modified GCE exhibited more positive potential and higher current density (0.53 V, 1.3 ± 0.2 mA cm^{-2}) for ORR than that obtained from 6 nm Pt nanoparticles (0.44 V, 0.8 ± 0.1 mA cm^{-2}) (Figure 7b) and bulk Pt (0.40 V, 0.7 ± 0.1 mA cm^{-2}) (Figure 7c), indicating that the as-prepared 3D DPNs showed higher electrocatalytic activity than that of the 6 nm Pt nanoparticles and bulk Pt. Furthermore, the mass current densities per unit mass of platinum were calculated at the oxidative peak positions of the 3D DPNs (0.53 V) and 6 nm Pt nanoparticles (0.44 V) in ORR. The mass-normalized activities were evaluated to be 16.0 ± 2 mA $mg^{-1}$and 11.6 ± 1 mA mg^{-1} for the 3D

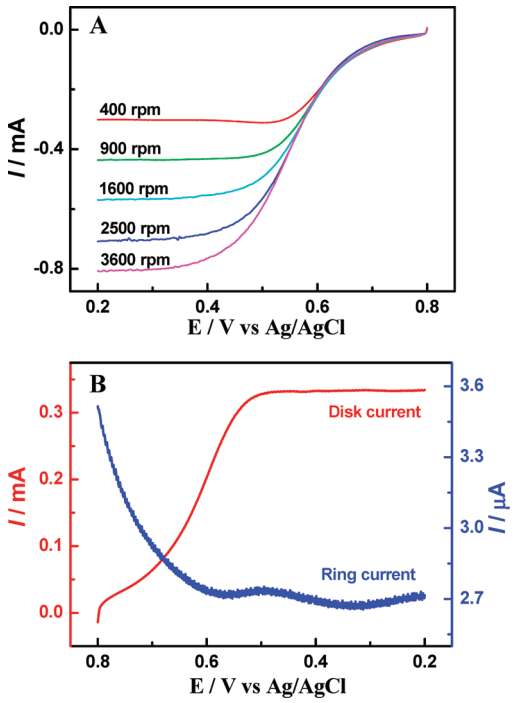

Figure 8. (A) Current−potential curves of O_2 reduction at a rotating disk electrode catalyzed by the 3D DPNs with different rotating rate in O_2-saturated 0.5 M H_2SO_4 solution. The scan rate was 50 mV s^{-1}. (B) Current−potential curves of O_2 reduction at a rotating ring-disk electrode catalyzed by the 3D DPNs in O_2-saturated 0.5 M H_2SO_4 solution; the potential of the ring electrode was maintained at 1.0 V; the rotation rate was 500 rpm, and the scan rate was 50 mV s^{-1}.

DPNs and 6 nm Pt nanoparticles, respectively. The specific structural features of the 3D DPNs, possessing of abundances of corner and edge sites, might be the reason for facilitating the ORR, compared with solid 6 nm Pt nanoparticles. It has been testified that the presence of a large number of edge and corner atoms holds the key to improving the catalytic performance of nanostructured platinum.[4b,21,24] Besides, the reduction potential (0.53 V) of ORR observed at the 3D DPNs modified GCE was significantly more positive than that of the other Pt-based electrodes.[20a,25] The voltammetric results clearly demonstrated as-prepared 3D DPNs were favorable for ORR with low overpotential.

The additional important index for ORR is the four-electron electroreduction of dioxygen to water, which is the reaction greatly pursued by scientists in view of its important application in fuel cells. So, the 3D DPNs were further investigated by RDE and RRDE experiments. Depicted in Figure 8A were the current−potential curves of ORR at a RDE catalyzed by the 3D DPNs with different rotating rate in O_2-saturated 0.5 M H_2SO_4 solution. The corresponding Levich and Koutecky−Levich plots were also obtained.[25e] From the slope of

(23) Guo, S.; Dong, S.; Wang, E. *Chem. Eur. J.* **2008**, *14*, 4689.

(24) Bratlie, K. M.; Lee, H.; Komvopoulos, K.; Yang, P. D.; Somorjai, G. A. *Nano Lett.* **2007**, *7*, 3097.

(25) (a) Ye, H.; Crooks, R. M. *J. Am. Chem. Soc.* **2005**, *127*, 4930. (b) Jin, Y. D.; Shen, Y.; Dong, S. J. *J. Phys. Chem. B* **2004**, *108*, 8142. (c) Shen, Y.; Liu, J. Y.; Wu, A. G.; Jiang, J. G.; Bi, L. H.; Liu, B. F.; Li, Z.; Dong, S. J. *Langmuir* **2003**, *19*, 5397. (d) Zhai, J. F.; Huang, M. H.; Zhai, Y. M.; Dong, S. J. *J. Chem. Mater.* **2008**, *18*, 923. (e) Huang, M. H.; Shao, Y.; Sun, X. P.; Chen, H. J.; Liu, B. F.; Dong, S. J. *Langmuir* **2005**, *21*, 323.

the Koutecky−Levich plot, the n (the electron-transfer number) value was evaluated to be about 4 for the 3D DPNs modified electrode. The electrocatalytic ability of the 3D DPNs for four-electron electroreduction of dioxygen was further testified by RRDE investigation. In RRDE investigation, the disk potential was scanned from +0.8 to +0.2 V, whereas the ring potential was kept at +1.0 V to oxidize the H_2O_2 generated by the O_2 reduction at the disk electrode. Figure 8B showed the voltammetric curves for dioxygen reduction recorded at the RRDE with the 3D DPNs immobilized on the electrode surface. As shown in Figure 8B, a large disk current was obtained and almost negligible ring current was observed. The ratio of the ring to disk current, I_R/I_D, was 0.008 (at 0.3 V) for the 3D DPNs. From the ratio of the I_R/I_D, the electron-transfer number (n) was calculated to be 3.92 according to the equation $n = 4-2(I_R/I_DN)$,[25e] which was consistent with that acquired from the RDE investigation. Taking into account that the rates of H_2O_2 and H_2O production are I_R/N and $I_D - I_R/N$, respectively, the formation efficiency of H_2O ($P_{(H2O)}$) could be estimated as follows[20b]

$$P_{(H_2O)} = \frac{N(I_D/I_R)-1}{N(I_D/I_R)+1}$$

Also from the value of I_R/I_D, 0.008, the efficiency of H_2O formation for the 3D DPNs amounted to 99.7%, suggesting that the as-prepared 3D DPNs electrocatalyst reduced dioxygen predominantly by four electrons to H_2O.

Recently, direct methanol fuel cells (DMFCs) have been intensely pursued because of their numerous advantages including high energy density, the ease of handling liquid, low operating temperatures, and their possible applications to micro fuel cells.[26] The performance of fuel cells, such as DMFCs, is known to be strongly dependent on the electrocatalytic materials used. Accordingly, for the best DMFC performance, it is essential to develop good electrocatalytic nanomaterials for exploring the performance of the methanol electrocatalytic oxidation. The electrocatalytic properties of the 3D DPNs toward the methanol oxidation reaction were furthermore tested and compared with approximately 6 nm Pt nanoparticles and bulk Pt electrode in 0.5 M H_2SO_4 solution containing 1 M methanol.

As shown in Figure 9, bare GCE had no electrocatalytic activity toward the oxidation of methanol (Figure 9d) and remarkable catalytic current was observed when the 3D DPNs modified GCE was used (Figure 9a), indicating that the notable electrocatalytic behavior was ascribed to the ability of the 3D DPNs. The onset potential of the electrocatalytic behavior was around 0.44 V (vs Ag/AgCl). The peak current densities at about 0.68 V in the forward sweep and at 0.50 V in the backward sweep were attributed to methanol electrooxidation at the 3D DPNs. The ECAS normalized activity of the 3D DPNs, as

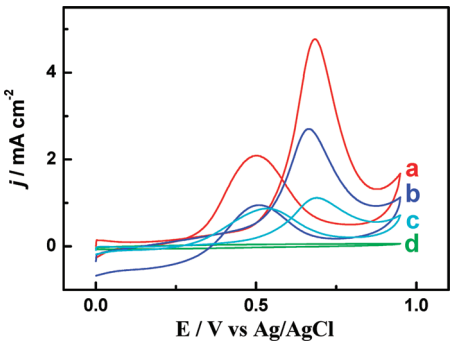

Figure 9. ECAS-normalized CVs displaying the catalyzed oxidation of methanol by using (a) 3D DPNs and (b) 6 nm Pt nanoparticles modified GCE, (c) bulk Pt electrode, and (d) bare GCE, respectively, in 0.5 M H_2SO_4 solution containing 1 M methanol. The scan rate was 50 mV s^{-1}.

recorded by the peak current density in the forward scan at 0.68 V, was 4.8 ± 0.3 mA cm^{-2}. For comparison, the ECAS normalized activities of 6 nm Pt nanoparticles and bulk Pt electrode were also measured to be 2.7 ± 0.2 mA cm^{-2} and 1.1 ± 0.2 mA cm^{-2}, respectively. Mass-normalized activity is an important parameter to evaluate the activity of surface atoms and the Pt utilization.[2e] Mass-normalized activities were also evaluated for the 3D DPNs and 6 nm Pt nanoparticles by using the peak current at 0.68 V, and the values were 104.4 ± 2 mA $mg^{-1}$and 50.5 ± 4 mA mg^{-1}, respectively. The mass-normalized activity of the 3D DPNs, 104.4 ± 2 mA mg^{-1}, was a little lower than that of the Pt nanonetworks (124.7 mA mg^{-1}) and higher than that of Pt nanosponges (57 mA mg^{-1}).[17e] It is widely accepted that the activity of catalysts depends on the physical and chemical nature of active surface atoms, which is sensitive to the adsorbed species.[2e] Considering the particular structure of the 3D DPNs, the favorable electrocatalytic ability might be ascribed to higher surface-to-volume ratios, enough absorption sites, and surface permeability compared with solid nanospheres (e.g., 6 nm Pt nanoparticles). It should be noted, in chronoamperometry measurements at 0.6 V, the as-prepared 3D DPNs exhibited quickly current decays during the initial period and decreased by 5% within 1 min, similar to the observations reported for similar Pt nanodendrites prepared by galvanic replacement reactions.[17e] The reason might be ascribed to the formation of intermediate species (e.g., CO_{ads}).[17e] The specific structural features of the 3D DPNs described herein offered favorable abilities for diverse applications in which platinum is required to be in low-density, high surface area form.

4. Conclusions

A very simple and efficient wet chemical route to straightforward synthesis of well-dispersed 3D DPNs at high yield was proposed. As-prepared 3D DPNs were shown to be active as nanoelectrocatalyst for the reduction of dioxygen and oxidation of methanol. The advantages of the proposed approach to synthesize 3D DPNs are obvious. First, this approach is very simple. The "one-step synthesis" conforms to this trend to make the synthesis process easy and widely feasible. Second, no organic

(26) Hyeon, T.; Han, S. J.; Sung, Y.; Park, K. W.; Kim, Y. W. *Angew. Chem., Int. Ed.* **2003**, *42*, 4352.

solvents, templates or ion replacements are involved. Third, very mild temperature is enough for the wet chemical synthesis and the high temperature is freed. Furthermore, the demonstrated route can be scaled up readily.

Acknowledgment. We sincerely thank Dr. Y. Nemoto for TEM studies and Dr. N. Suzuki for N_2 adsorption measurement of the 3D DPNs. This work was supported by World Premier International Research Center (WPI) Initiative on "Materials Nanoarchitectonics", Ministry of Education, Culture, Sports, Science and Technology (MEXT), Japan. The present study is in part supported by a Grant-in-Aid for Scientific Research (19850031) from Japan Society for the Promotion of Science (JSPS) and the Murata Science Foundation.